Origin of liquid fragility

Chae Woo Ryu [1] and Takeshi Egami [1,2,3,*]

[1]*Department of Materials Science and Engineering, University of Tennessee, Knoxville, Tennessee 37996, USA*
[2]*Materials Sciences and Technology Division, Oak Ridge National Laboratory, Oak Ridge, Tennessee 37831, USA*
[3]*Department of Physics and Astronomy, University of Tennessee, Knoxville, Tennessee 37996, USA*

(Received 2 July 2020; accepted 12 October 2020; published 26 October 2020)

Liquid fragility characterizes how steeply the viscosity of a glass-forming liquid decreases with increasing temperature above the glass transition. It is one of the most fundamental properties of a liquid, with high importance for science and application. Yet, its origin is unclear. Here we show that it is directly related to the structural coherence of the medium-range order (MRO) in liquid defined by the decay of the pair-distribution function with distance. The MRO can also be evaluated from the first peak of the structure function determined by x-ray or neutron diffraction, and it is a measure of the cooperativity of atomic motion in a diffusive event in supercooled liquids. These findings shed light on the mechanism of atomic transport in supercooled liquids.

DOI: 10.1103/PhysRevE.102.042615

I. INTRODUCTION

When a liquid is cooled its viscosity increases rapidly with decreasing temperature. If the liquid is supercooled by avoiding crystallization, the viscosity becomes so high that the liquid behaves like a solid, and this state is called a glass. Such a change in the viscous behavior is called the glass transition, which is defined by viscosity reaching 10^{13} poise ($=10^{12}$ Pa · sec) [1]. The temperature dependence of viscosity, η, just above the glass transition temperature, T_g, is quantified as fragility [2,3],

$$m = \left.\frac{d\log\eta(T)}{d(T_g/T)}\right|_{T=T_g}. \tag{1}$$

Liquids with larger values of m are characterized as fragile, whereas those with smaller values of m approaching 17 are called strong. Variation in fragility results in huge difference in viscosity in supercooled liquids by many orders of magnitude, and therefore it is important for applications and for other properties such as glass-forming ability. However, why fragility varies from one liquid to the other is not well understood. Angell suggested that it is related to the magnitude of the jump in specific heat at T_g, and thus to the covalency of atomic bonds [2]. It was then found that fragility is related to vibrational properties, such as the sound velocity [4,5] and finally to the ratio between the shear modulus, G, and the bulk modulus, B, and thus to Poisson's ratio [6]. However, different groups of liquids, such as metallic liquids and molecular liquids, appear to show different relationships [7,8]. In addition, it was proposed that anharmonicity was responsible for fragility [9,10], and the temperature variation of the liquid structure was found to be linked to fragility [11–13]. While these observations are important, they fall short of pointing to a universal microscopic mechanism that controls fragility.

*egami@utk.edu

II. RESULTS

A. Medium-range order and fragility

The structure of liquid and glass is usually described in terms of the atomic pair-distribution function (PDF), $g(r)$, which shows the distribution of distances between two atoms. For liquids it gives a snapshot, because atoms are moving all the time. The PDF is the same-time correlation function, and it can be obtained by experiment through Fourier-transformation of the structure function, $S(Q)$, where Q is the momentum exchange in scattering, determined by x-ray or neutron diffraction [14,15]. The PDF of liquid and glass has a relatively sharp first peak which depicts the nearest-neighbor atoms, followed by higher-order broader peaks. As predicted by Ornstein and Zernike [16] the PDF decays with distance beyond the first peak as

$$G(r) = 4\pi r\rho_0[g(r) - 1] = G_0(r)\exp(-r/\xi_s), \tag{2}$$

where ρ_0 is the atomic number density, ξ_s is the structural coherence length which characterizes the medium-range order (MRO), and $G_0(r)$ is the reduced PDF of the ideal glass state [17]. The MRO does not represent structural order at the atomic level. It embodies correlations among coarse-grained atomic density fluctuations, rather than detailed atomic correlations which depend on chemical nature of atomic bonds [18].

The MRO is more clearly observed for metallic liquids and glasses for which the structural unit is an atom, whereas it is less visible for complex molecular liquids and glasses. We determined the value of ξ_s for the metallic alloy liquids we studied by x-ray diffraction and molecular dynamics (MD) simulation [17], and compared them against the experimentally determined values of fragility m. We found a strong correlation between m and the value of ξ_s at T_g, $\xi_s(T_g)$,

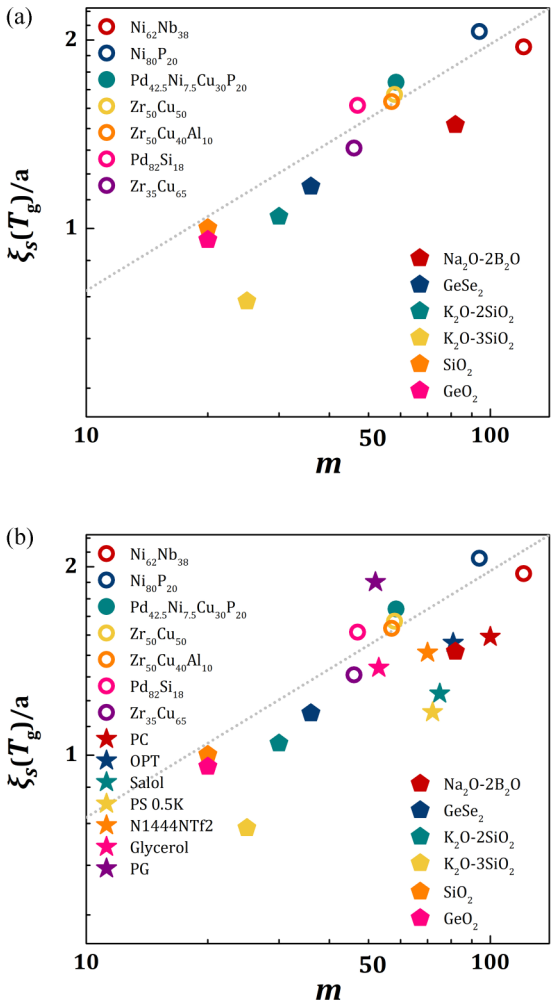

FIG. 1. (a) Correlation between fragility, m, and normalized structural coherence length, $\xi_s(T_g)/a$, for metallic and chalcogenide liquids, shown in a log-log scale. The dashed line is a fit only for metallic liquids. (b) The same plot with added data for organic liquids.

normalized by the average nearest-neighbor distance, a,

$$\left(\frac{\xi_s(T_g)}{a}\right)^{d_c} = \frac{m}{m_{0,c}}, \tag{3}$$

where $d_c = 2.54 \pm 0.6$ and $m_{0,c} = 17.9$, as shown in Fig. 1(a) and discussed in the Appendix.

We then examined the data for network glasses in the literature. For network glasses the first sharp diffraction peak (FSDP) characterizes the MRO. The value of ξ_s can be determined from the width of the FSDP as $\xi_s = 2/\Delta Q_{\mathrm{FSDP}}$, where ΔQ_{FSDP} is the FWHM of the FSDP, assuming the Lorentzian peak shape. As for the value of a we used $a = 3\pi/2Q_{\mathrm{FSDP}}$, where Q_{FSDP} is the position of the FSDP in Q. As suggested in Ref. [19] the value of a thus defined is close to the cation-cation distance in oxides. As shown in Fig. 1(a) the data for the FSDP of oxides and chalcogenides line up well with those for metallic liquids, except for K_2O-$3SiO_2$. Some organic liquids also show FSDP in the diffraction pattern. We studied the FSDP data shown in Refs. [13,20]. The data for organic glasses and other network glasses exhibit surprisingly similar

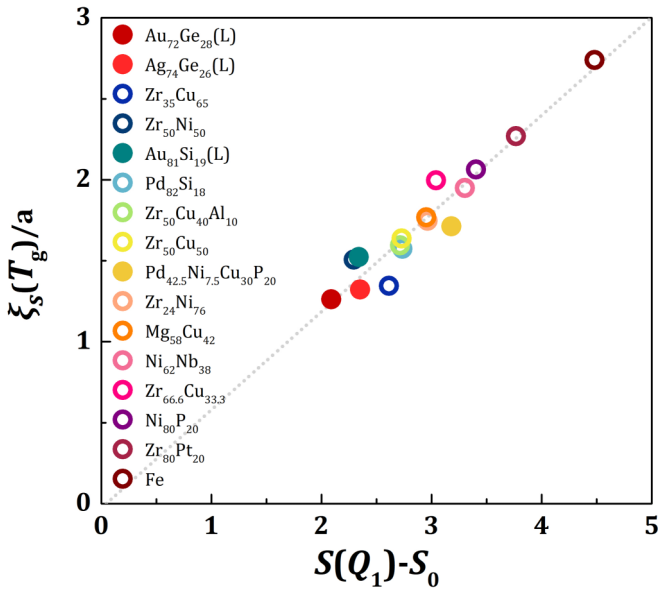

FIG. 2. Correlation between $S(Q_1) - S_0$ at T_g, with $S_0 = 0.325$ and $\xi_s(T_g)/a$ for metallic liquids.

correlation as metallic glasses as shown also in Fig. 1(b), although the data are more scattered.

For many liquids and glasses the data on $\xi_s(T_g)$ are not available. However, for metallic glasses $\xi_s(T_g)$ is related to the height of the first peak of $S(Q)$ at T_g, $S(Q_1)$, where Q_1 is the position of the first peak [17]. As shown in Fig. 2 $\xi_s(T_g)/a$ is proportional to $S(Q_1) - S_0$, where S_0 (=0.325) represents the effect of the overlap with the second peak. In Fig. 3 we plot $S(Q_1) - S_0$ against m in logarithmic scale including those liquids and glasses for which $\xi_s(T_g)$ is not known but the values of $S(Q_1)$ and m are known, as shown in Table II. Strong correlations are seen even though the data were collected from

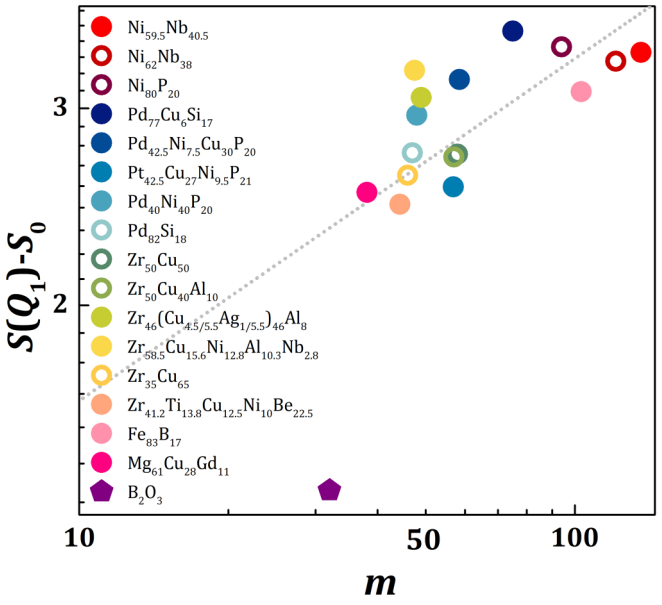

FIG. 3. Correlation between and m and $S(Q_1) - S_0$ at T_g, with $S_0 = 0.325$, for metallic liquids and B_2O_3.

a variety of sources, except for the data point for B_2O_3. It is most likely that the relation between $\xi_s(T_g)$ and $S(Q_1) - S_0$ for the network glasses is different from that for metallic glasses [21]. If we exclude the data for B_2O_3, we find

$$[S(Q_1, T_g) - S_0]^{d_s} = \frac{m}{m_{0,s}}, \tag{4}$$

with $d_s = 3.27 \pm 0.92$ and $m_{0,s} = 2.0$. The details of the data are given in Table I in the Appendix.

The data shown in Figs. 1–3 include both those by simulation (open symbols) and those by experiment (closed symbols). Despite the different natures of the data they appear to overlap well. The cooling rates for simulation are much higher than those by experiment by many orders of magnitude, resulting in less relaxed states. The measured $S(Q)$ includes x-ray or neutron scattering factors for which elements weigh differently. However, the effects of structural relaxation on $S(Q)$ are minor [22], and the MRO is rather insensitive to chemistry [18]. For these reasons, these factors apparently give rise only to slightly increased scatter in the data, and the underlying correlations are robust and less affected by these factors. We believe that this robustness justifies the mixed use of simulation and experimental data for $\xi_s(T_g)$ and $S(Q_1) - S_0$ together with the experimentally derived values of m. The data shown in Figs. 1 and 3 show considerable scatter. The scatter partially reflects the difficulty of determining the value of m by experiment. It is often derived by thermal measurement of the relaxation time rather than by the direct measurement of viscosity. The value differs considerably from one literature to the other even for the same liquid.

Earlier studies suggested strong correlations between fragility and the temperature dependencies of $S(Q_1)$ [12,17] and the coherence length determined by the FSDP [13]. These results point to the structural origin of fragility. However, the observations shown in Figs. 1 and 3 go much further, and they indicate that the magnitude of $\xi_s(T_g)$ itself is related to fragility. As fragility is defined at T_g it is reasonable that fragility is controlled by the structure at T_g, characterized by the structural coherence.

B. Cooperativity of dynamics

For metallic glasses the structural coherence length ξ_s appears to be directly related to viscosity. We may express viscosity in terms of the temperature-dependent activation energy, $E_a(T)$,

$$\eta(T) = \eta_\infty \exp\left(\frac{E_a(T)}{k_B T}\right). \tag{5}$$

We found earlier [17] that for $Pd_{42.5}Ni_{7.5}Cu_{30}P_{20}$ liquid just above T_g, $E_a(T)$ is related to ξ_s by

$$E_a(T) = E_0\left(\frac{\xi_s(T)}{a}\right)^{d_E}, \tag{6}$$

where $d_E = 3$, a value similar to those of d_c and d_s. Given the uncertainty in the experimental data, we consider small differences among d_c, d_s, and d_E insignificant and assume $d_c = d_s = d_E = 3$ to simplify the discussion. Now, to confirm Eq. (6) by experiment, $g(r)$ and viscosity need to be measured over a significant temperature range just above T_g. It is very difficult to carry out such measurements for metallic glasses because they crystallize easily above T_g. So far it has been done only for a very stable $Pd_{42.5}Ni_{7.5}Cu_{30}P_{20}$ liquid. But, if Eq. (6) can be generalized for other liquids this implies that both fragility and the activation energy are proportional to the coherence volume, $V_c = [\xi_s(T)]^3$. The number of atoms in the coherence volume is given by

$$n_c(T_g) = \rho_0[\xi_s(T_g)]^3 = \frac{6 f_p}{\pi}\left(\frac{\xi_s(T_g)}{a}\right)^3, \tag{7}$$

where f_p is the atomic packing fraction which is similar for most metallic glasses ($\sim$0.7). As shown in Figs. 4(a)–4(c) the plot of $n_c(T_g)$ against m shows good correlation with $n_c(T_g) = m/m_n$, with $m_n = 10.7 \pm 1.1$ for metallic liquids, $m_n = 7.4 \pm 0.4$ for organic liquids, and 7.3 ± 1.2 for network liquids. The overall fit indicates $m_n = 8.7 \pm 0.6$. It is interesting to note that organic liquids show much better correlations in this plot than in Fig. 1(b), revealing the underlying correlation which is not obvious just by comparing m and $\xi_s(T_g)$. Now, for a very strong liquid ($m = 17$), $n_c(T_g)$ is close to 2, the number of atoms involved in cutting one bond as expected for strong network liquid. Therefore, it is reasonable to regard $n_c(T_g)$ as representing the number of atoms involved in overcoming the activation barrier. The results in Fig. 4 suggest that fragility is a measure of cooperativity in the activation dynamics of viscosity.

Through MD simulations [23], an inelastic x-ray scattering measurement on water [24], and an inelastic neutron scattering measurement on metallic liquid [25], it has been shown that liquid viscosity at high temperatures is controlled by cutting of just one atomic bond around each atom. More specifically, the Maxwell relaxation time, $\tau_M = \eta/G_\infty$, where G_∞ is the high-frequency shear modulus, is equal to $\tau_{\rm LC}$, the time for an atom to lose one nearest-neighbor atom, above T_A. The T_A is the viscosity crossover temperature above which viscosity shows the Arrhenius temperature dependence [26]. Above T_A the phonon propagation length, $c_T\tau_M$, where c_T is the transverse sound velocity, becomes shorter than a, so that the structure changes before the phonon travels from one atom to the nearest neighbor [23]. Consequently, atoms cannot influence each other much through phonons, and the dynamics becomes mostly local. The Maxwell relaxation time is equal to the stress correlation time via the fluctuation-dissipation theorem [27]. Cutting one bond alters the atomic-level stresses strongly enough to terminate local stress correlation and thus controls viscosity [23]. Below T_A, however, the dynamics is more cooperative, and the ratio $\tau_M/\tau_{\rm LC}$ increases with decreasing temperature [23,25]. This results in the increase in ξ_s, which is related to the increase in $E_a(T)$ through Eq. (6).

III. DISCUSSION

A. Cooperativity and fragility

There are several possible reasons why n_c, the number of atoms involved in local plastic deformation, varies from one composition to the other. The first is the openness of the structure. When the structure is open as in covalent network

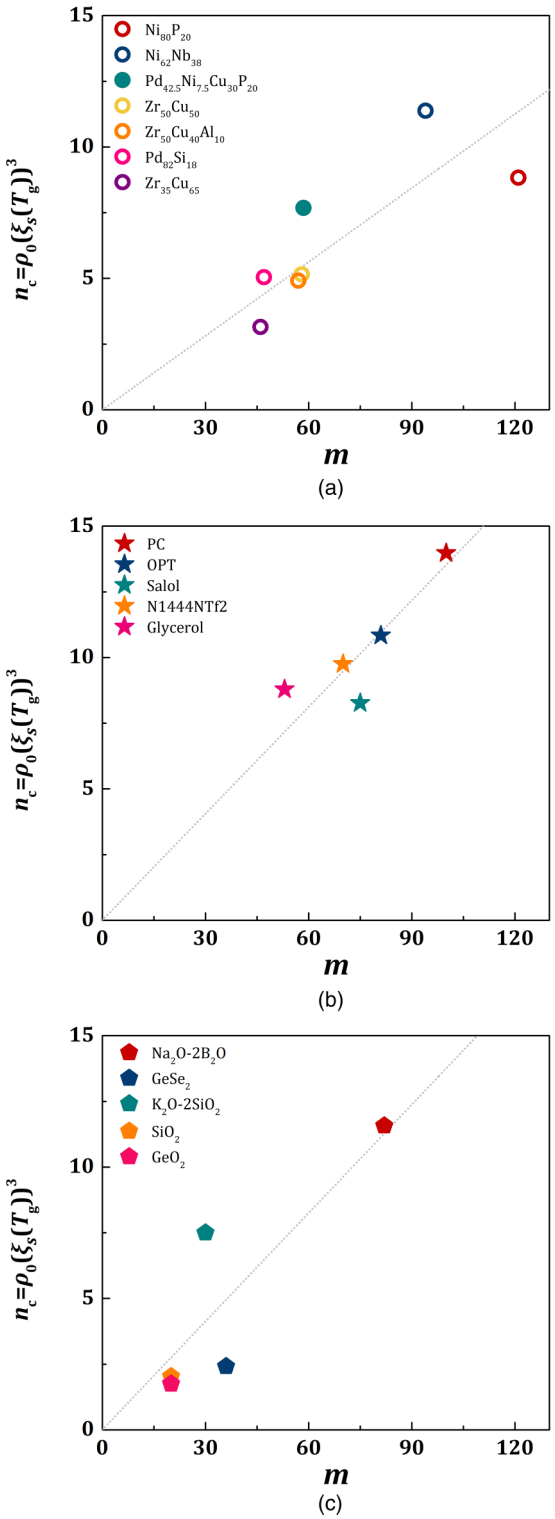

FIG. 4. Correlation between m and $\rho_0[\xi_s(T_g)]^3$. (a) Data for metallic liquids, (b) for organic liquids, and (c) for network liquids. Dashed lines are linear fits for each group.

glasses local bond breaking causes distortion in the network structure, but other bonds are likely to remain unbroken. Thus, the number of atoms involved in transport and deformation is small, so that the system is strong. However, in the close-packed structure as in metallic glasses local bond breaking will induce local rearrangement of a larger number of atoms, five atoms on average at the saddle point of the potential energy landscape (PEL) [28,29]. For this reason, the number of atoms involved is larger than two, rendering the system fragile.

The second possible reason is the ease of compression. The smallest most prevalent form of local plastic deformation in close-packed liquids is the bond exchange involving 4 atoms in two dimensions (Fig. 5) and 5 atoms in three dimensions. In this process in order to preserve a constant area (volume) at the saddle point atomic bonds need to be compressed. Such compression is difficult for strongly repulsive potentials (strong anharmonicity [9,10]), and not at all possible for hard spheres. This volume expansion at the saddle point can induce other plastic events nearby, resulting in the increased number of atoms involved in the process.

In our view, however, the most important factor is the structural ideality. We have shown that the values of $\xi_s(T_g)$ and $S(Q_1) - 1$ at T_g are strongly related to the shape of the first peak of $S(Q)$ [30]. When the peak shape is closer to the Lorentzian the peak height is high and ξ_s is long, whereas when it is more Gaussian the peak height is low and ξ_s is short. Because the Ornstein-Zernike decay of the PDF, Eq. (2), results in the Lorentzian peak shape, having a Lorentzian peak is evidence of a more "ideal" structure. For this reason, the values of $\xi_s(T_g)$ and $S(Q_1) - 1$ at T_g are good measures of the "ideality" of the structure [30]. By extrapolating ξ_s to infinity we defined the ideal glass structure which has long-range density correlations without periodicity in the structure [17]. The result presented here implies that the fragility is directly related to the ideality of the structure; the more ideal, the more fragile. Indeed the w_L/w_G ratio, where w_L and w_G are the Lorentzian and Gaussian widths in the Voigt fit for the first peak of $S(Q)$, is related to $m^{1/3}$ as shown in Fig. 6 in the Appendix. The principal factor which induces deviations from ideality is covalency in bonding. The Ornstein-Zernike theory of the PDF presumes spherical interatomic potential [16]. Strongly directional covalent bonds would compete against the Ornstein-Zernike correlation, and cause deviations from the exponential decay behavior [30]. The importance of covalency in liquid fragility was already suggested by Angell [2], but the mechanism was unclear. Here covalency is linked to fragility through the loss of structural coherence and ideality.

B. Structural defects

The observation that fragility is related to the medium-range order and thus to the atomic cooperativity in deformation has wider implications. In crystals atomic transport is possible only through the motion of structural defects, such as vacancies and interstitial defects. This led to the idea that atomic transport in liquid is also controlled by defect-like objects, such as free volume [31], cooperatively rearranging regions [32], and shear transformation zone under stress [33]. However, whereas in a crystal defects are topologically protected by the lattice and preserve their identity after motion, the same does not apply for liquid and glass. For this reason, today these defects in glass are considered to be

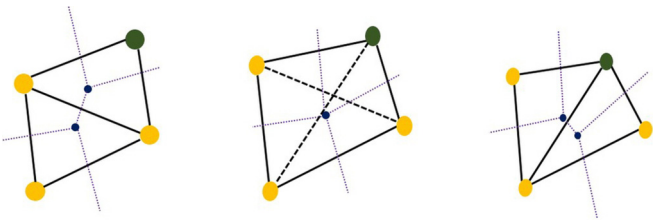

FIG. 5. Bond exchange process in 2D.

transient; they do not preexist and disappear after the action [34–36].

The result shown here advances this argument even further. The coherence length ξ_s describes the volume average of the structure in equilibrium, not the structure of defects, suggesting that the atomic transport in liquid is controlled by bulk structure but not by defects. In liquids, during the process of atomic migration the neighboring atoms rearrange themselves significantly, so that the final structure after a diffusional step is vastly different from the prior initial structure. A schematic one-dimensional picture of the PEL may give an impression that the pathway from one PEL minimum to the next is predetermined. However, the reality is very different and highly stochastic. When the system rises to the top of the saddle point it loses the memory of the initial state [37], as if it melts for a very short time at the saddle point [38]. Therefore, the pathway up to the saddle point is decoupled from the pathway down to the next minimum, and the potential energy of the final state is very different from that of the initial state. Even though the propensity to start deformation depends on the initial state, once an atomic migration step is initiated the details of the initial state are unimportant and forgotten. What is important is how the system reacts to local atomic displacement by rearranging the neighboring atoms. We believe that this is the reason why the activation energy is proportional to the coherence volume through Eq. (6), and to the number of atoms involved. That is why the extent of atomic correlations in the bulk, the MRO, is the most critical property for atomic transport as demonstrated here. Various models of defects may depict the dynamic transient state near the saddle point, but their dynamics must be controlled by the bulk MRO.

IV. CONCLUSION

Liquid fragility is one of the most fundamental properties of a liquid. Yet, its origin has been controversial. In this work we show that it is directly related to the structural coherence length of the medium-range order (MRO) in liquid at the glass transition. The MRO is defined by the decay of the pair-distribution function with distance in the Ornstein-Zernike form. The MRO can also be evaluated from the first peak of the structure function determined by x-ray or neutron diffraction. The MRO is a measure of the cooperativity of atomic motion, because the activation energy of viscosity is proportional to the number of atoms in the coherence volume, n_c. We show that n_c is proportional to the fragility coefficient, m, although the proportionality constant varies slightly among different classes of liquids. The results shed light on the mechanism of atomic transport in supercooled liquids.

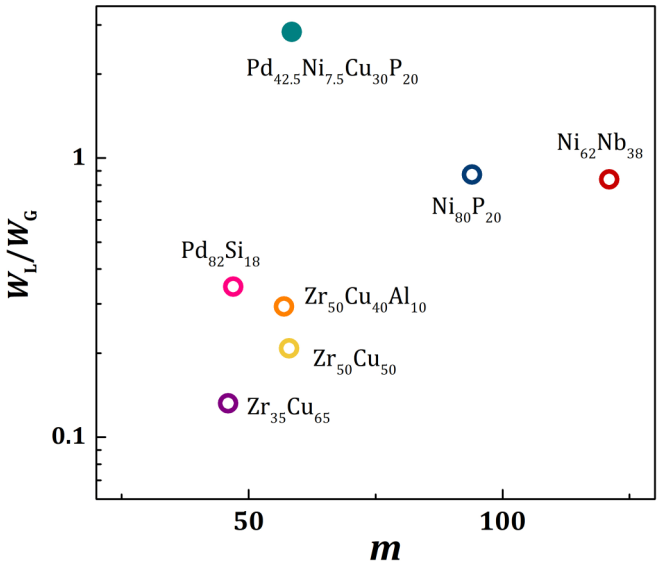

FIG. 6. Correlation between w_L/w_G and m for various metallic alloy liquids.

ACKNOWLEDGMENTS

The authors thank J. S. Langer and A. P. Sokolov for informative discussion. This work was supported by the US Department of Energy, Office of Sciences, Basic Energy Science, Materials Sciences and Engineering Division.

APPENDIX

1. Power law for fragility and coherence length

The power law for fragility and coherence length is given in Table I.

2. The values of T_g, ξ_s, and $S(Q_1)$ for various liquids and glasses

These values are given in Table II.

TABLE I. Power law for fragility and coherence length. A linear function, $f = ax + b$, was fitted to y for the data given in the table. The power was given by $d_c = \sqrt{d_{c1}d_{c2}} = 2.54$ and $d_s = \sqrt{d_{s1}d_{s2}} = 3.27$.

x	y	a	d_c or d_s	Δd
$\log(m)$	$\log[\xi_s(T_g)/a]$	d_{c1}	2.24	0.53
$\log[\xi_s(T_g)/a]$	$\log(m)$	$1/d_{c2}$	2.87	0.68
$\log(m)$	$\log[S(Q_1) - S_0]$	d_{s1}	4.74	1.33
$\log[S(Q_1) - S_0]$	$\log(m)$	$1/d_{s2}$	2.25	0.63

TABLE II. Values of T_g, ξ_s, and $S(Q_1)$ for various liquids and glasses.

	T_g (K)	ξ_s	$S(Q_1)$	m	Comments
GeO_2	818	3.03		20	ξ_s calculated from Ornstein-Zernike
	[39]	[40]		[39]	equation [40] at RT.
$GeSe_2$	687	4.17		36	ξ_s calculated from Ornstein-Zernike
	[42]	[40]		[41,42]	equation [40] at RT.
					average value of fragility [41,42].
SiO_2	1500	3.13		20	ξ_s calculated from 1/HWHM
	[39]	[20]		[39]	[20] at RT.
B_2O_3	554		1.69	32	$S(Q_1)$ measured T: RT.
	[39]		[43,44]	[39]	here we used the neutron scattering data.
Salol	220	4.55		75	ξ_s calculated from 1/HWHM
	[13]	[13]		[13]	[13] at $0.9T_g$.
Na_2O-$2B_2O_3$	748	5.00		82	ξ_s calculated from 1/HWHM
	[13]	[13]		[13]	[13] at $0.9T_g$.
OTP	246	4.88		81	ξ_s calculated from 1/HWHM
	[13]	[13]		[13]	[13] at $0.9T_g$.
N1444NTf2	205	4.71		70	ξ_s calculated from 1/HWHM
	[13]	[13]		[13]	[13] at $0.9T_g$.
K_2O-$2SiO_2$	768	5.13		30	ξ_s calculated from 1/HWHM
	[13]	[13]		[13]	[13] at $0.9T_g$.
K_2O-$3SiO_2$	760	4.17		25	ξ_s calculated from 1/HWHM
	[13]	[13]		[13]	[13] at $0.9T_g$.
PS 0.5 K (polystyrene)	253	4.00		72	ξ_s calculated from 1/HWHM
	[13]	[13]		[13]	[13] at $0.9T_g$.
Glycerol	190	4.17		53	ξ_s calculated from 1/HWHM
	[13]	[13]		[13]	[13] at $0.9T_g$.
PC (propylene carbonate)	158	5.13		100	ξ_s calculated from 1/HWHM
	[13]	[13]		[13]	[13] at $0.9T_g$.
PG (propylene glycol)	160	6.06		52	ξ_s calculated from 1/HWHM
	[13]	[13]		[13]	[13] at $0.9T_g$.
$Pd_{42.5}Ni_{7.5}Cu_{30}P_{20}$	573	4.74	3.51	58.5	
				[45]	
$Pd_{82}Si_{18}$	762	4.25	3.06	47	
				[46]	
$Zr_{50}Ni_{50}$	724	4.00	2.62		
$Zr_{24}Ni_{76}$	734	4.54	3.29		
$Zr_{35}Cu_{65}$	691	3.70	2.94	46	
				[47]	
$Zr_{50}Cu_{50}$	671	4.51	3.05	58	
				[48,49]	
$Zr_{66.6}Cu_{33.3}$	675	5.71	3.37		
$Zr_{50}Cu_{40}Al_{10}$	779	4.48	3.04	57	
				[50]	
$Zr_{80}Pt_{20}$	901	6.84	4.09		
$Ni_{62}Nb_{38}$	970	4.97	3.63	121	
				[51]	
$Ni_{80}P_{20}$	546	5.04	3.73	94	
				[49]	
$Mg_{58}Cu_{42}$	545	4.78	3.28		
Fe	950	6.97	4.81		
$Au_{81}Si_{19}$		4.31	2.66		ξ_s measured T: 665 K.
		[52]	[52]		
$Au_{72}Ge_{28}$		3.48	2.41		ξ_s measured T: 666 K.
		[52]	[52]		
$Ag_{74}Ge_{26}$		3.66	2.68		ξ_s measured T: 976 K.
		[52]	[52]		
$Pt_{42.5}Cu_{27}Ni_{9.5}P_{21}$	514		2.88	56.9	$S(Q_1)$ measured T: 514 K.
	[54]		[53]	[54]	
$Zr_{41.2}Ti_{13.8}Cu_{12.5}Ni_{10}Be_{22.5}$	613		2.79	44.4	$S(Q_1)$ measured T: 610 K.
	[55]		[56]	[55]	

TABLE II. (*Continued.*)

	T_g (K)	ξ_s	$S(Q_1)$	m	Comments
$Zr_{58.5}Cu_{15.6}Ni_{12.8}Al_{10.3}Nb_{2.8}$	666		3.57	47.5	$S(Q_1)$ measured T: 673 K.
	[55]		[57]	[55]	
$Pd_{40}Ni_{40}P_{20}$	570		3.28	48	$S(Q_1)$ measured T: 560 K.
	[58]		[58]	[45]	
$Mg_{61}Cu_{28}Gd_{11}$	422		2.85	38.1	$S(Q_1)$ measured T: RT.
	[59]		[60]	[59]	
$Fe_{83}B_{17}$	760		3.43	103	$S(Q_1)$ measured T: RT.
	[51]		[61]	[51]	
$Ni_{59.5}Nb_{40.5}$	890		3.69	136	$S(Q_1)$ measured T: 890 K.
	[62]		[62]	[8]	
$Zr_{46}(Cu_{4.5/5.5}Ag_{1/5.5})_{46}Al_8$	703		3.39	49	$S(Q_1)$ measured T: RT.
	[63]		[63]	[63]	
$Pd_{77}Cu_6Si_{17}$	653		3.84	75	$S(Q_1)$ measured T: 653 K.
	[64]		[64]	[8]	

3. Deformation unit

In liquid the most frequently observed smallest unit of local deformation is a bond-exchange process in which an atomic bond is cut and a new bond is formed in the immediate vicinity [29,65,66]. In two dimensions it involves four atoms (Fig. 5), whereas in three dimensions five atoms are involved [26].

4. Correlation with ideality

Together with the values of $\xi_s(T_g)$ and $S(Q_1) - 1$ at T_g the w_L/w_G ratio, where w_L and w_G are the Lorentzian and Gaussian widths in the Voigt fit for the first peak of $S(Q)$, is a good measure of ideality of the liquid structure. Figure 6 shows good correlation between w_L/w_G and m, except for $Pd_{42.5}Ni_{7.5}Cu_{30}P_{20}$.

[1] P. G. Debenedetti and F. H. Stillinger, Nature (London) **410**, 259 (2001).
[2] C. A. Angell, Science **267**, 1924 (1995).
[3] C. A. Angell, J. Non-Cryst. Solids **73**, 1 (1985).
[4] A. P. Sokolov, E. Rössler, A. Kisliuk, and D. Quitmann, Phys. Rev. Lett. **71**, 2062 (1993).
[5] T. Scopigno, G. Ruocco, F. Sette, and G. Monako, Science **302**, 849 (2003).
[6] V. N. Novikov and A. P. Sokolov, Nature (London) **431**, 961 (2004).
[7] G. P. Johari, Philos. Mag. **86**, 1567 (2006).
[8] V. N. Novikov and A. P. Sokolov, Phys. Rev. B **74**, 064203 (2006).
[9] C. M. Roland, S. Hensel-Bielowka, M. Paluch, and R. Casalini, Rep. Prog. Phys. **68**, 1405 (2005).
[10] J. Krausser, K. H. Samwer, and A. Zaccone, Proc. Natl. Acad. Sci. USA **112**, 13762 (2015).
[11] Y. Zhao, X. Bian, X. Qin, J. Qin, and X. Hou, Phys. Lett. A **367**, 364 (2007).
[12] N. A. Mauro, M. Blodgett, M. L. Johnson, A. J. Vogt, and K. F. Kelton, Nat. Commun. **5**, 4616 (2014).
[13] D. N. Voylov, P. J. Griffin, B. Mercado, J. K. Keum, M. Nakanishi, V. N. Novikov, and A. P. Sokolov, Phys. Rev. E **94**, 060603(R) (2016).
[14] P. A. Egelstaff, *An Introduction to the Liquid State*, 2nd ed. (Oxford University Press, New York, 1991).
[15] N. H. March and M. P. Tosi, *Introduction to Liquid State Physics* (World Scientific, Singapore, 2002).
[16] L. S. Ornstein and F. Zernike, Proc. K. Ned. Akad. Wet. (KNAW) **17**, 793 (1914).
[17] C. W. Ryu, W. Dmowski, K. F. Kelton, G. W. Lee, E. S. Park, J. R. Morris, and T. Egami, Sci. Rep. **9**, 18579 (2019).
[18] T. Egami, Front. Phys. **8**, 50 (2020).
[19] P. S. Salmon and A. Zeidler, J. Stat. Mech. (2019) 114006.
[20] Y. Onodera, S. Kohara, S. Tahara, A. Masuno, H. Inoue, M. Shiga, A. Hirata, K. Tsuchiya, Y. Hiraoka, I. Obayasi, K. Ohara, A. Mizuno, and O. Sakata, J. Ceram. Soc. Jpn. **127**, 853 (2019).
[21] R. Shi and H. Tanaka, Sci. Adv. **5**, eaav3194 (2019).
[22] T. Egami, J. Mater. Sci. **13**, 2587 (1978).
[23] T. Iwashita, D. M. Nicholson, and T. Egami, Phys. Rev. Lett. **110**, 205504 (2013).
[24] T. Iwashita, B. Wu, W.-R. Chen, S. Tsutsui, A. Q. R. Baron, and T. Egami, Sci. Adv. **3**, e1603079 (2017).
[25] R. Ashcraft, Z. Wang, D. L. Abernathy, T. Egami, and K. F. Kelton, J. Chem. Phys. **152**, 074506 (2020).
[26] D. Kivelson, S. A. Kivelson, X. Zhao, Z. Nussinov, and G. Tarjus, Physica A **219**, 27 (1995).
[27] J.-P. Hansen and I. R. McDonald, *Theory of Simple Liquids* (Academic Press, Elsevier, Amsterdam, 2006).
[28] Y. Fan, T. Iwashita, and T. Egami, Nat. Commun. **5**, 5083 (2014).
[29] J. Bellissard and T. Egami, Phys. Rev. E **98**, 063005 (2018).
[30] C. W. Ryu, W. Dmowski, and T. Egami, Phys. Rev. E **101**, 030601(R) (2020).
[31] M. H. Cohen and D. Turnbull, J. Chem. Phys. **31**, 1164 (1959).
[32] G. Adam and J. H. Gibbs, J. Chem. Phys. **43**, 139 (1965).
[33] A. S. Argon, Acta Metall. **27**, 47 (1979).
[34] M. L. Falk and J. S. Langer, Phys. Rev. E **57**, 7192 (1998).
[35] J. S. Langer, Phys. Rev. E **70**, 041502 (2004).

[36] C. A. Schuh, T. C. Hufnagel, and U. Ramamurty, Acta Mater. **55**, 4067 (2007).
[37] Y. Fan, T. Iwashita, and T. Egami, Nat. Commun. **8**, 15417 (2017).
[38] J. Ding, L. Li, N. Wang, L. Tian, M. Asta, R. O. Ritchie, and T. Egami (unpublished).
[39] R. Böhmer, K. L. Ngai, C. A. Angell, and D. J. Plazek, J. Chem. Phys. **99**, 4201 (1993).
[40] S. P. Salmon, J. Phys.: Condens. Matter **19**, 455208 (2007).
[41] K. Gunasekera, B. Bhosle, P. Boolchand, and M. Micoulaut, J. Chem. Phys. **139**, 164511 (2013).
[42] P. Lucas, G. J. Coleman, M. V. Rao, A. N. Edwards, C. Devaadithya, S. Wei, A. Q. Alsayoud, B. G. Potter, K. Muralidharan, and P. A. Deymier, J. Phys. Chem. B **121**, 11210 (2017).
[43] A. Zeidler, K. Wezka, D. A. J. Whittaker, P. S. Salmon, A. Baroni, S. Klotz, H. E. Fischer, M. C. Wilding, C. L. Bull, M. G. Tucker, M. Salanne, G. Ferlat, and M. Micoulaut, Phys. Rev. B **90**, 024206 (2014).
[44] V. V. Brazhkin, Y. Katayama, K. Trachenko, O. B. Tsiok, A. G. Lyapin, E. Artacho, M. Dove, G. Ferlat, Y. Inamura, and H. Saitoh, Phys. Rev. Lett. **101**, 035702 (2008).
[45] H. Kato, T. Wada, M. Hasegawa, J. Saida, A. Inoue, and H. S. Chen, Scr. Mater. **54**, 2023 (2006).
[46] N. Chen, Y. Li, and K. F. Yao, J. Alloys Compd. **504**, S211 (2010).
[47] A. Jaiswal, T. Egami, K. F. Kelton, K. S. Schweizer, and Y. Zhang, Phys. Rev. Lett. **117**, 205701 (2016).
[48] K. Russew, L. Stojanova, S. Yankova, E. Fazakas, and L. K. Varga, J. Phys.: Conf. Ser. **144**, 012094 (2009).
[49] W. L. Johnson, J. H. Na, and M. D. Demetriou, Nat. Commum. **7**, 10313 (2016).
[50] J. C. Qiao, R. Casalini, and J. M. Pelletier, J. Non-Cryst. Solids **407**, 106 (2015).
[51] T. Komatsu, J. Non-Cryst. Solids **185**, 199 (1995).
[52] P. Chirawatkul, A. Zeidler, P. S. Salmon, S. Takeda, Y. Kawakita, T. Usuki, and H. E. Fischer, Phys. Rev. B **83**, 014203 (2011).
[53] O. Gross, N. Neuber, A. Kuball, B. Bochtler, S. Hechler, M. Frey, and R. Busch, Commun. Phys. **2**, 83 (2019).
[54] O. Gross, B. Bochtler, M. Stolpe, S. Hechler, W. Hembree, R. Busch, and I. Gallino, Acta Mater. **132**, 118 (2017).
[55] I. Gallino, Entropy **19**, 483 (2017).
[56] S. Wei, F. Yang, J. Bednarcik, I. Kaban, O. Shuleshova, A. Meyer, and R. Busch, Nat. Commun. **4**, 2083 (2013).
[57] M. Stolpe, I. Jonas, S. Wei, Z. Evenson, W. Hembree, F. Yang, A. Meyer, and R. Busch, Phys. Rev. B **93**, 014201 (2016).
[58] S. Lan, Y. Ren, X. Y. Wei, B. Wang, E. P. Gilbert, T. Shibayama, S. Watanabe, M. Ohnuma, and X. L. Wang, Nat. Commun. **8**, 14679 (2017).
[59] Q. Zheng, J. Xu, and E. Ma, J. Appl. Phys. **102**, 113519 (2007).
[60] W. B. Zhang, X. D. Wang, Q. G. Kong, H. J. Ruan, X. B. Zuo, Y. Ren, Q. P. Cao, H. Wang, D. W. Zhang, and J. Z. Jiang, J. Phys. Chem. C **123**, 27868 (2019).
[61] D. M. Paul, R. A. Cowley, W. G. Stirling, N. Cowlam, and H. A. Davies, J. Phys. F: Met. Phys. **12**, 2687 (1982).
[62] N. A. Mauro, M. L. Johnson, J. C. Bendert, and K. F. Kelton, J. Non-Cryst. Solids **362**, 237 (2013).
[63] Q. K. Jiang, X. D. Wang, X. P. Nie, G. Q. Zhang, G. Q., H. Ma, H. J. Fecht, J. Bendnarcik, H. Franz, Y. G. Liu, Q. P. Cao, and J. Z. Jiang, Acta Mater. **56**, 1785 (2008).
[64] A. J. Vogt, Ph.D. thesis, Washington University in St. Louis, 2014.
[65] Y. Suzuki, J. Haimovich, and T. Egami, Phys. Rev. B **35**, 2162 (1987).
[66] T. Iwashita and T. Egami, Phys. Rev. Lett. **108**, 196001 (2012).